

Time-dependent analysis of spherical accretion onto black holes

L. Zampieri,¹ J. C. Miller,^{1,2} and R. Turolla³

¹ International School for Advanced Studies (S.I.S.S.A.), Via Beirut 2–4, 34013 Trieste, Italy

² Nuclear and Astrophysics Laboratory, University of Oxford, Keble Road, Oxford OX1 3RH, England

³ Department of Physics, University of Padova, Via Marzolo 8, 35131 Padova, Italy

Accepted ... Received ... ; in original form 1995 June 5

ABSTRACT

Results are presented from a time-dependent, numerical investigation of spherical accretion onto black holes, within the framework of relativistic radiation hydrodynamics. We have studied the stability of self-consistent, stationary solutions of black hole accretion with respect to thermal and radiative perturbations and also the non-linear evolution of unstable, high temperature models, heated by the hard radiation produced by the accretion flow itself in the inner region near to the horizon. In some cases, a hydrodynamic shock forms at around 10^3 – 10^4 Schwarzschild radii, where Compton heating exceeds radiative cooling. The calculations were made using a suitably designed radiation hydrodynamics code, in which radiative transfer is handled by means of the PSTF moment formalism and which contains an original treatment of the radiation temperature equation.

Key words: accretion, accretion discs – hydrodynamics – instabilities – methods: numerical – radiative transfer.

1 INTRODUCTION

Stationary, spherical accretion onto black holes is a well-known and extensively studied topic. Starting from the seminal paper by Bondi (1952), many papers have been devoted to the analysis of spherical accretion under a variety of conditions, mainly in order to obtain a definite estimate of the efficiency of the process. In contrast with accretion onto neutron stars, the efficiency is not fixed by the requirement that all the kinetic energy of the accreting gas must be converted into radiation, since no rigid surface exists which can stop the flow. Matter can cross the horizon carrying a substantial fraction of the gravitational potential energy liberated and the efficiency of the process is determined solely by the effectiveness of the radiative processes in converting the internal energy of the accreting gas into radiation, as first noted by Shvartsman (1971). As shown by many authors (see e.g. Michel 1972; Novikov & Thorne 1973; Blumenthal & Mathews 1976; Begelman 1978; Brinkmann 1980), the flow properties are fixed once the accretion rate is specified, so that stationary solutions can be completely characterized by their position in the (\dot{m}, l) plane, where \dot{m} and l are, respectively, the accretion rate and luminosity in Eddington units. Stationary spherical accretion onto black holes was investigated in detail by Nobili, Turolla & Zampieri (1991, hereafter NTZ); Fig. 1 shows the (\dot{m}, l) diagram for the complete set of their solutions. At low accretion rates ($\dot{m} < 1$), spherical accretion is very inefficient in converting gravitational energy into radiation since the density is

too low for cooling processes to be effective; the emitted luminosity is also very low (lower branch in Fig. 1, hereafter the LL branch). These models are essentially adiabatic and have very high temperatures (see also Shapiro 1973a). In this regime, the only possibility for increasing the efficiency of the accretion process is related to the presence of magnetic fields, which can cause strong dissipation (e.g. through reconnection of field lines) and induce strong emission of synchrotron radiation (Shapiro 1973b; Mészáros 1975). Sofel (1982) studied in some detail the transition from the optically thin regime to the optically thick one: as \dot{m} increases, the cooling processes become more effective and the gas temperature decreases, causing in turn a decrease in the total emitted luminosity (with a local minimum at around $\dot{m} \simeq 0.1$). For higher values of the accretion rate, free-free absorption is no longer negligible and the gas becomes optically thick in the inner region near to the horizon of the black hole. The temperature increases because heating exceeds cooling and also the luminosity rises since radiation is in LTE with the gas in the inner core. Preliminary investigations of spherical accretion in the diffusion regime were made by Tamazawa et al. (1974), Maraschi, Reina & Treves (1974), Kafka & Mészáros (1976), Vitello (1978), Begelman (1979), Gillman & Stellingwerf (1980) and Freihofer (1981), while a complete treatment was finally given by Flammang (1982, 1984), who showed the existence of a subcritical point related to the equation for the radiative luminosity. When $\dot{m} > 1$, the inner core starts to be optically thick to electron scattering as well. In these conditions, a trapping radius ap-

pears (Rees 1978; Begelman 1978), below which photons are advected into the black hole, since their outward diffusion velocity is smaller than the inward velocity of the accretion flow. This makes the process less efficient and the rate of increase of luminosity with \dot{m} becomes slower. The stationary, hypercritical regime has been investigated by Blondin (1986).

For $3 \lesssim \dot{m} \lesssim 100$, there is also another class of solutions, characterized by having high temperatures and luminosities (upper branch in Fig. 1, hereafter the HL branch). These are dominated by the effects of comptonization which keeps the gas and radiation temperatures almost equal in the inner part of the flow where the density is sufficiently high to make the Compton parameter very large. In the intermediate region between 10^2 and $10^5 r_g$ (where r_g is the Schwarzschild radius of the black hole), Compton heating dominates and the only competitive cooling mechanism is free-free emission. The first authors to investigate the possible existence of high luminosity solutions were Wandel, Yahil & Milgrom (1984) and Park (1990a,b), who performed a detailed study of spherical accretion for a large range of accretion rates and considered also a two-temperature model with pair production. High luminosity stationary solutions have relatively high efficiency and appear to exist only for a very definite range of accretion rates. Already in 1976, Ostriker and collaborators (Ostriker et al. 1976) pointed out that, because of the non-local nature of comptonization, the heating produced in the flow by the hard radiation coming from the inner region can increase the gas temperature in such a way that the internal energy density becomes larger than the gravitational energy density and the accretion process is then stopped. This effect is called *preheating*. Later on, Cowie et al. (1978), Shull (1979), Stellingwerf & Buff (1982) and Krolik & London (1983) showed that preheating is very important in placing limits on the region of parameter space within which HL solutions for black hole accretion can exist, although the strength of preheating is reduced if Compton cooling is taken into account (see e.g. Bisnovatyi-Kogan & Blinnikov 1980). As shown by NTZ, preheating *at* the sonic point for the matter prevents the existence of high luminosity solutions with $\dot{m} \lesssim 3$, while preheating *within* the sonic radius prevents the existence of stationary solutions for $\dot{m} \gtrsim 100$.

The stability of these solutions remains a completely open question and the main goal of the present paper is to study this. The first attempt to investigate the stability of isothermal accretion was made by Stellingwerf & Buff (1978) using an Eulerian scheme, based on an extension of the Henyey relaxation method. They found that transonic accretion is quite stable. By means of a general relativistic analytical calculation, Moncrief (1980) showed that, for isentropic flows, no unstable normal modes exist which extend outside the sound horizon. The first studies including the heating and cooling terms due to the presence of the radiation field (Cowie et al. 1978; Stellingwerf & Buff 1982; Stellingwerf 1982) were devoted to analysing the effect of preheating on the stability of the accretion flow and to defining the region of the (\dot{m}, l) plane where the existence of stationary solutions is not allowed. In particular, Stellingwerf (1982) presented a local stability analysis of optically thin, X-ray heated accretion flows and showed that, for sufficiently high luminosities, a finite amplitude drift in

stability can develop, due to the form of the free-free cooling function, causing a time-dependent behaviour of the solution on a time-scale ranging between a day and a few tens of days. Krolik & London (1983) used the WKB method to derive the dispersion relation for modes coupling density, temperature and velocity perturbations in an optically thin, accreting gas and found that, although stationary solutions with high temperature and luminosity can exist, heating of the gas inside the sonic radius leads to the onset of a thermal instability in a large region of the (\dot{m}, l) plane. Gilden & Wheeler (1980) and Vitello (1984) investigated time-dependent, optically thick accretion within the framework of General Relativity, treating the radiation field in the diffusion approximation and using two different numerical schemes: a Lagrangian hydrodynamic code in the first case and a Linearized Block Implicit Algorithm in the second one. They found that, within this approximation, no matter which initial conditions the code started from, convergence toward stationary LL solutions was rapidly achieved, showing that they are intrinsically stable. Finally, NTZ, using an argument originally suggested by Nobili, Calvani & Turolla (1985) and based on Prigogine's criterion, argued that HL solutions might be unstable because of the large value of the entropy production rate.

Despite the fact that the stationary problem has been extensively investigated, mainly for shedding light on the efficiency of the radiation generation, we think that several aspects require further consideration such as, for instance, investigating the stability properties of the high luminosity solutions and searching for the existence and non-linear evolution of possible heated or shocked models. In the present paper we present an analysis of the stability and time-dependent behaviour of the solutions for spherical accretion onto black holes within the framework of general relativistic radiation hydrodynamics. We adopt the conventions that Greek indices run from 0 to 3 and covariant derivatives are denoted with a semi-colon; a spacelike signature $(-, +, +, +)$ is used.

2 THEORY

In this section we review the derivation of the equations of relativistic radiation hydrodynamics in spherical symmetry for a self-gravitating matter fluid which is interacting with radiation. A complete treatment of this subject was recently presented by Rezzolla & Miller (1994) in connection with the cosmological quark-hadron transition (see also Schmid-Burgk 1978, Mihalas & Mihalas 1984 and Park 1993 for a discussion of the equations of radiation hydrodynamics in spherical flows). Since the source terms which account for the emission and absorption of photons are more easily written in the reference frame comoving with the gas, this will be our fiducial frame and u^α will denote its 4-velocity. In this frame the energy and momentum conservation equations can be obtained by projecting the 4-divergence of the stress-energy tensor of the matter plus radiation fluid along u^α and orthogonal to it, giving

$$u_\alpha (T_M^{\alpha\beta} + T_R^{\alpha\beta})_{;\beta} = 0, \quad (1)$$

$$h_{\gamma\alpha} (T_M^{\alpha\beta} + T_R^{\alpha\beta})_{;\beta} = 0, \quad (2)$$

Figure 1

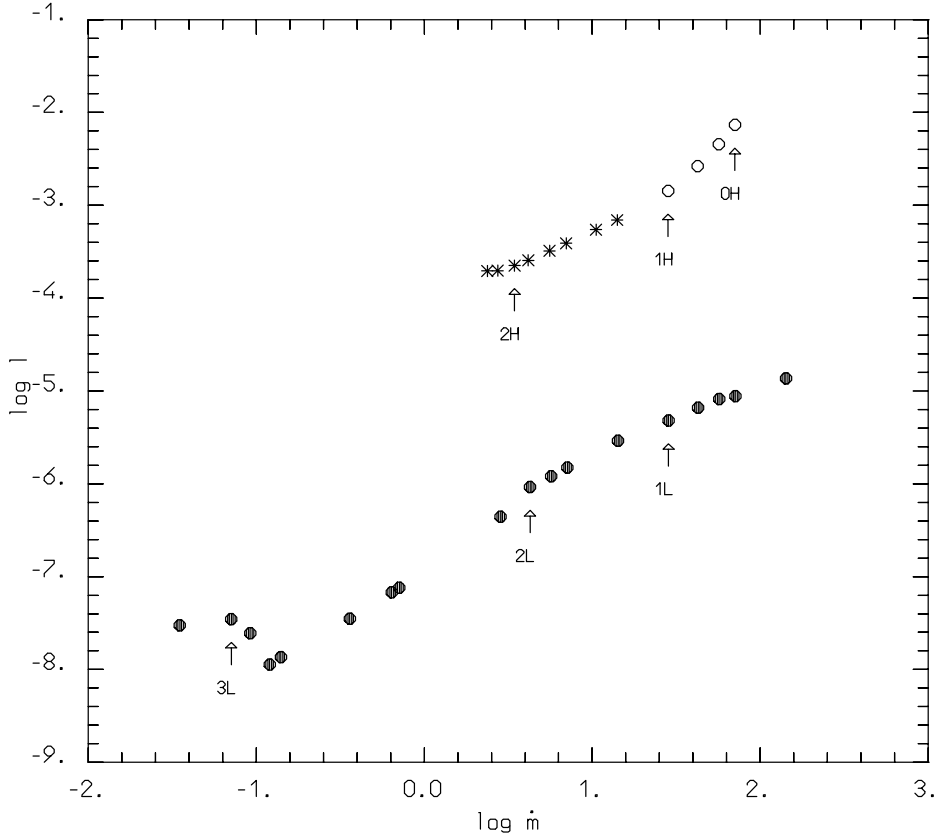


Figure 1. The (\dot{m}, l) diagram for the complete set of stationary solutions found by NTZ (circles). Also shown are the 6 initial models whose relevant parameters are listed in table 1. Filled circles mark the stable LL stationary solutions, while open circles denote the unstable HL models. Asterisks indicate the low \dot{m} HL solutions, which might still be unstable, but on much longer time-scales.

where $h_{\gamma\alpha} = g_{\gamma\alpha} + u_{\gamma}u_{\alpha}$ is the projection tensor orthogonal to the 4-velocity and

$$T_M^{\alpha\beta} = (e + p) u^{\alpha} u^{\beta} + p g^{\alpha\beta}, \quad (3)$$

$$T_R^{\alpha\beta} = \mathcal{M} u^{\alpha} u^{\beta} + 2\mathcal{M}^{(\alpha} u^{\beta)} + \mathcal{M}^{\alpha\beta} + \frac{1}{3} \mathcal{M} h^{\alpha\beta} \quad (4)$$

are the matter and radiation stress-energy tensors, respectively; e and p are the energy density and pressure of the gas. This system of equations must be supplemented with the rest-mass conservation equation

$$(\rho u^{\alpha})_{;\alpha} = 0, \quad (5)$$

where ρ is the rest-mass density of the matter measured in the comoving frame. In equation (4) the stress-energy tensor of the radiation field is expressed in terms of the Projected Symmetric Trace-Free (PSTF) moments (Thorne 1981)

$$\mathcal{M}^{\alpha_1 \dots \alpha_k} = \frac{1}{c} \left(\int I n^{\alpha_1} \dots n^{\alpha_k} d\Omega \right)^{Trace-Free}, \quad (6)$$

where $I = I(x^{\alpha}, p^{\alpha})$ is the specific intensity of the radiation field and n^{α} is the unit vector which gives the direc-

tion of propagation of a photon as seen in the rest frame of the fiducial observer u^{α} . Integration is over solid angle in the projected space and ‘‘Trace-Free’’ denotes the consequence of the usual tensor operation. By definition, the PSTF moments are symmetric tensors which lie entirely in the projected space and represent the relativistic analogue of the classical moments of the specific intensity (see e.g. Chandrasekhar 1960). In terms of PSTF moments, I can be written as

$$I = c \sum_{k=0}^{\infty} \frac{(2k+1)!!}{4\pi k!} \mathcal{M}^{\alpha_1 \dots \alpha_k} n_{\alpha_1} \dots n_{\alpha_k}. \quad (7)$$

The specific intensity obeys the general relativistic equation of radiative transfer

$$2 \frac{dN}{dl} = S, \quad (8)$$

where $N = (c^2/2h)(I/\nu^3)$ is the photon occupation number ($\nu = cu^{\alpha}p_{\alpha}/h$ is the photon frequency measured in the comoving frame), l is a non-affine parameter along the photon trajectory in phase-space and S is a source function which describes the effects of the interaction between mat-

ter and radiation, its actual form depending on the radiative processes which are considered. The moments of the source function, $S^{\alpha_1 \dots \alpha_k}$, can be defined in analogy with equation (6). If there is no interaction, $S = 0$ and N is conserved along each photon trajectory. Moment equations can be obtained from equation (8) by inserting the expansion (7) for I (and the equivalent one for S) and taking the PSTF part (i.e. projecting orthogonal to u^α , removing the trace and performing the symmetrization); this gives rise to an infinite hierarchy of differential equations.

Finally, in order to calculate self-consistently the metric tensor $g^{\alpha\beta}$ which describes the geometry of the space-time, we need to solve the Einstein Field Equations for the system

$$R^{\alpha\beta} - \frac{1}{2}g^{\alpha\beta}R = \frac{8\pi G}{c^4} (T_M^{\alpha\beta} + T_R^{\alpha\beta}) . \quad (9)$$

In spherical symmetry we can define a local orthonormal frame comoving with the flow as $\{\mathbf{e}_{\hat{0}}, \mathbf{e}_{\hat{r}}, \mathbf{e}_{\hat{\theta}}, \mathbf{e}_{\hat{\phi}}\}$, with $\mathbf{e}_{\hat{0}} = \mathbf{u}$, $\mathbf{e}_{\hat{r}}$ being in the radial direction and $\mathbf{e}_{\hat{\theta}}, \mathbf{e}_{\hat{\phi}}$ being orthogonal to each other and to $\mathbf{e}_{\hat{r}}$. Since in this case I and S are invariant under rotations of the photon direction n^α about $\mathbf{e}_{\hat{r}}$, it is possible to show that all of the components of each PSTF moment of rank k can be evaluated in the comoving frame as functions of the radial one

$$w_k \equiv \mathcal{M}^{\hat{r} \dots \hat{r}} = 2\pi \frac{k!(2k+1)}{(2k+1)!!} \frac{1}{c} \int I P^k(\mu) d\mu , \quad (10a)$$

$$s_k \equiv \mathcal{S}^{\hat{r} \dots \hat{r}} = 2\pi \frac{k!(2k+1)}{(2k+1)!!} \frac{h}{c^3} \int \nu^3 S P^k(\mu) d\mu , \quad (10b)$$

where $P^k(\mu)$ is the Legendre polynomial of order k , $\mu = n^{\hat{r}}$ and \hat{a} denotes the $\mathbf{e}_{\hat{a}}$ component. In particular

$$\mathcal{M} = w_0 , \quad (11)$$

$$\mathcal{M}^\alpha = w_1 e_{\hat{r}}^\alpha , \quad (12)$$

$$\mathcal{M}^{\alpha\beta} = w_2 \left(e_{\hat{r}}^\alpha e_{\hat{r}}^\beta - \frac{1}{2} e_{\hat{\theta}}^\alpha e_{\hat{\theta}}^\beta - \frac{1}{2} e_{\hat{\phi}}^\alpha e_{\hat{\phi}}^\beta \right) . \quad (13)$$

In the following, we will be interested only in frequency-integrated moments and we will use w_k to denote the integral over ν of $w_k(\nu)$. It is easy to see that w_0 is the radiation energy density and cw_1 is the radial component of the radiative flux.

We next introduce the spherically symmetric, comoving-frame line element

$$ds^2 = -a^2 c^2 dt^2 + b^2 d\mu^2 + r^2 (d\theta^2 + \sin^2 \theta d\varphi^2) , \quad (14)$$

where t and μ are the Lagrangian time and the comoving radial coordinate (taken to be the rest mass contained within a comoving spherical shell), r is the Eulerian radial coordinate and a and b are two functions of t and μ which need to be computed. The complete system of radiation hydrodynamic equations (1), (2) and (5) along with the Einstein Field Equations (9) can be cast in the form (Rezzolla & Miller 1994)

$$e_t - h\rho_t + acs_0 = 0 \quad \text{Energy equation} , \quad (15)$$

$$u_t + ac \left[\frac{\Gamma}{b} \left(\frac{p_\mu + bs_1}{\rho h} \right) + \frac{4\pi Gr}{c^4} \left(p + \frac{1}{3} w_0 + w_2 \right) + \frac{GM}{c^2 r^2} \right] = 0 \quad \text{Euler equation} , \quad (16)$$

$$\begin{aligned} \frac{(\rho r^2)_t}{\rho r^2} + ac \left(\frac{u_\mu - 4\pi Gbrw_1/c^4}{r_\mu} \right) \\ = 0 \quad \text{Continuity equation} , \end{aligned} \quad (17)$$

$$b = \frac{1}{4\pi r^2 \rho} , \quad (18)$$

$$\frac{(ah)_\mu}{ah} + \frac{h\rho_\mu - e_\mu + bs_1}{h\rho} = 0 , \quad (19)$$

$$M_\mu = \frac{4\pi r^2 r_\mu}{c^2} \left(e + w_0 + \frac{u}{\Gamma} w_1 \right) , \quad (20)$$

where

$$u = \frac{r_t}{ac} \quad (21)$$

is the radial component of the fluid 4-velocity measured in the fixed Eulerian frame, $\Gamma = (1 + u^2 - 2GM/c^2r)^{1/2} = r_\mu/b$ is the general relativistic analogue of the Lorentz factor, M represents the effective gravitational mass (for black hole + gas + radiation) contained within radius r and $h = (e + p)/\rho$ is the specific enthalpy. Here, the subscripts t and μ denote partial derivatives with respect to the corresponding variables and s_0 and s_1 are the radial moments of the source function S . In spherical symmetry and with the line-element (14), the first two moment equations can be written (Thorne 1981, equation [5.10c])

$$\begin{aligned} \frac{1}{b^{4/3} r^{8/3}} (w_0 b^{4/3} r^{8/3})_t + \frac{c}{ab r^2} (w_1 a^2 r^2)_\mu \\ + \left(\frac{b_t}{b} - \frac{r_t}{r} \right) w_2 - acs_0 = 0 , \end{aligned} \quad (22a)$$

$$\begin{aligned} \frac{1}{b^2 r^2} (w_1 b^2 r^2)_t + \frac{c}{3a^3 b} (w_0 a^4)_\mu \\ + \frac{c}{b r^3} (w_2 a r^3)_\mu - acs_1 = 0 . \end{aligned} \quad (22b)$$

In equations (22) w_0 and w_1 have the dimensions of energy density and cs_0 and cs_1 are in units of $\text{erg cm}^{-3} \text{ s}^{-1}$. It is well-known that the moment equations form a recursive system of differential equations that is not closed. At any given order k_{max} it contains moments up to order k_{max+1} in the frequency-integrated case (and k_{max+2} in the frequency-dependent case). This means that, in order to use these equations for calculations, it is necessary to make some “ad hoc” assumption to close the system (see e.g. Fu 1987, Cernohorsky & Bludman 1994 and references therein) and this is usually done on physical grounds by introducing suitable closure functions which relate $w_{k_{max+1}}$ (and $w_{k_{max+2}}$ where necessary) to moments of lower order. Since the behaviour of all of the moments is known in the asymptotic limits (when the interaction between matter and radiation is either very strong or completely absent), it is sufficient to prescribe a reasonable smooth function that connects these two limits (see e.g. NTZ). Clearly uncertainties in this will introduce some error into the calculation of the lower order moments, whose magnitude will be dependent on the closure relation but turns out to be no larger than $\sim 15\%$ for the range of parameter values typical for real astrophysical flows (Turolla & Nobili 1988).

The radiation hydrodynamic equations (15)–(21), together with the first two moment equations (22) need to be

supplemented with the constitutive equations for the gas, the expressions for the source moments, a prescription for the closure function and suitable boundary conditions.

3 THE MODEL

In the following, we will consider spherical accretion of a self-gravitating hydrogen gas in the gravitational field of a non-magnetized, non-rotating black hole. The basic equations have been presented in the previous section; here we will specify all of the input physics (expressions for the source moments, equations of state, etc.) needed for solving the problem. Stationary, spherical accretion onto black holes has recently been investigated in detail by NTZ. The main goal of the present paper is to ascertain the stability properties of the solutions found by NTZ; in particular, we want to study the behaviour of the models in a certain range of accretion rates, for which both low and high luminosity solutions exist. To allow a direct comparison of our results with those of NTZ, we will adopt the same input physics which they considered, including the simplifying assumptions that Compton scattering can always be treated in the Kompaneets limit and that pair processes can be neglected. This turns out to be an excellent approximation for LL models while it becomes questionable in HL solutions where the gas temperature reaches $\sim 10^{10}$ K in the inner region. On the other hand, the work by Park (1990b) has shown that the inclusion of pair production and annihilation does not produce any dramatic changes.

If the dominant radiative processes are bound-free, free-free and isotropic scattering, the radial source moments s_0 and s_1 can be written (Thorne 1981; NTZ)

$$s_0 = \rho(\epsilon - k_0 w_0) + k_{es} \rho w_0 \frac{4k_B T}{m_e c^2} \left(1 - \frac{T_\gamma}{T}\right), \quad (23)$$

$$s_1 = -\rho k_1 w_1, \quad (24)$$

where $c\epsilon$ is the emissivity per unit mass per unit time, k_0 , k_1 and k_{es} are the absorption, flux-mean and scattering opacities, respectively, and T_γ is the radiation temperature, defined by

$$T_\gamma = \frac{1}{4k_B} \frac{\int_0^\infty h\nu w_0(\nu) d\nu}{\int_0^\infty w_0(\nu) d\nu}. \quad (25)$$

In equation (23) the second term on the right hand side accounts for the energy exchange between matter and radiation due to non-conservative scatterings and is obtained by integrating the Kompaneets equation over frequency and neglecting the non-linear term which describes induced emission. Since it is derived in the Fokker-Planck approximation, this term is certainly not adequate for describing the interaction between photons and electrons when the latter become relativistic, as happens in some of the solutions which we have computed. However, even in this case, the model can give a good qualitative indication of the correct results. We have expressed the emissivity using the interpolation of the cooling function Λ given by Stellingwerf & Buff (1982)

$$\epsilon = \frac{\rho\Lambda}{m_p^2 c}, \quad (26)$$

$$\Lambda = \left[(1.42 \times 10^{-27} T^{1/2} \beta_{rel} + 6.0 \times 10^{-22} T^{-1/2})^{-1} \right. \\ \left. + 10^{25} \left(\frac{T}{15,849 K} \right)^{-12} \right]^{-1} \text{erg cm}^3 \text{s}^{-1},$$

$$\beta_{rel} = (1 + 4.4 \times 10^{-10} T),$$

which includes bound-bound, free-bound, $e-p$ and $e-e$ bremsstrahlung for a pure hydrogen gas; the factor β_{rel} is a relativistic correction. Assuming LTE between emitters and absorbers, we can use the Kirchhoff law to obtain the Planck mean opacity, $k_P = \epsilon/a_R T^4$, where a_R is the blackbody radiation constant. Since the actual spectral distribution of w_0 cannot be computed here, we use k_P in place of the absorption opacity k_0 . The flux-mean opacity k_1 can be split into two terms: the first is the scattering opacity k_{es} and the second is the sum of the contributions from all of the other radiative processes; however, since k_{es} is always dominant for the range of densities and temperatures encountered in the present problem, we have approximated the additional term using the Rosseland mean k_R calculated taking into account only free-free processes

$$k_1 \simeq k_{es} + k_R, \quad (27)$$

$$k_R = 6.4 \times 10^{22} \rho T^{-7/2} \text{ cm}^2 \text{ g}^{-1}.$$

In the frequency-integrated transfer problem, the radiation temperature T_γ cannot be directly computed from its definition (equation [25]). However, since T_γ appears only in the term in s_0 which accounts for comptonization, it only becomes important when the energy exchange between matter and radiation due to non-conservative scatterings starts to be effective. In a medium at rest, the fractional change of the mean photon energy ($E = 4k_B T_\gamma$) because of scatterings with a thermal, non-relativistic distribution of electrons, follows the relation

$$\frac{dE}{E} = \frac{4k_B T}{m_e c^2} \left(\frac{E}{4k_B T} - 1 \right) \alpha d\tau,$$

(Rybicki & Lightman 1979, Wandel, Yahil & Milgrom 1984) where τ is the scattering depth, $4k_B T(E/4k_B T - 1)/m_e c^2$ is the mean energy change per scattering and $\alpha d\tau$ is the mean number of scatterings which a photon undergoes between τ and $\tau + d\tau$, with

$$\alpha = 1 \quad \text{for } \tau < 1,$$

$$\alpha = 2\tau \quad \text{for } \tau > 1.$$

From the computational point of view, it is convenient to write an equation for T_γ which is valid over all of the integration domain with continuous coefficients; for this reason the previous equation is usually written in the following form, which is an approximation near to $\tau \simeq 1$ (Park & Ostriker 1989; Park 1990a):

$$\frac{d \ln T_\gamma}{d \ln \tau} = 2Y_c \left(\frac{T_\gamma}{T} - 1 \right), \quad (28)$$

where $Y_c = 4k_B T \max(\tau, \tau^2)/m_e c^2$ is the Compton parameter. In stationary calculations, this equation has been used directly to give the variation of T_γ with r , at constant Eulerian time \tilde{t} , but for non-stationary flows it is not satisfactory to integrate it along the time-slice (i.e. at constant

Lagrangian time t) as this would imply an infinite speed of propagation of information. Instead, we apply it along the outward-pointing characteristics of the radiation field, $\mu_c(t)$ (defined from the moment equations [22]), and calculate the optical depth τ along the same lines using

$$\tau = \int_{\mu}^{\infty} k_{es} \rho b \Gamma d\mu. \quad (29)$$

This seems a reasonable choice because the radiation temperature is strictly related, by definition, to the radiation energy density and we expect that information will propagate along the characteristic lines of the radiation field. In this case it is not difficult to show (see the Appendix, equation [A5]) that

$$\frac{\partial T_{\gamma}}{\partial t} = -ac\Gamma v_c \left[\frac{2k_{es}\rho Y_c}{\tau} T_{\gamma} \left(\frac{T_{\gamma}}{T} - 1 \right) + \frac{1}{b\Gamma} \frac{\partial T_{\gamma}}{\partial \mu} \right], \quad (30)$$

where $v_c = b\dot{\mu}_c/ac$ is the characteristic velocity for the radiation field and $\dot{\mu}_c = d\mu_c/dt$. This is the actual form of the equation for T_{γ} used in our calculations. Equation (30) applies when comptonization is the dominant radiative process and also gives the correct behaviour (an outgoing radiation temperature wave) when non-conservative scattering becomes inefficient as long as true emission and absorption can be neglected. For the HL models, true absorption is never dominant and true emission is never likely to significantly affect T_{γ} and so the use of equation (30) is always satisfactory. For the LL models, true emission and absorption are dominant but in this case the second term on the right hand side of equation (23) is small compared with the other terms and an accurate evaluation of T_{γ} is no longer needed. The stationary limit of equation (30) (see again the Appendix, equation [A8]) is

$$\left(1 + \frac{u}{\Gamma v_c}\right) \frac{\partial T_{\gamma}}{\partial r} \Big|_{\tilde{t}} = -\frac{2k_{es}\rho Y_c}{\tau} T_{\gamma} \left(\frac{T_{\gamma}}{T} - 1 \right), \quad (31)$$

where the partial derivative is taken at constant Eulerian time \tilde{t} . In this form, the presence of a critical point where $u = -\Gamma v_c$ is made apparent. We note that this result is a consequence of the finite velocity of propagation in equation (30); in fact, as is well-known, the presence of critical points in the hydrodynamic equations for stationary flow is a relic of the characteristic velocity of the corresponding time-dependent equations. This result represents the main difference between the form of the T_{γ} equation used here and the one considered in all previous studies of this problem in the framework of black hole accretion (Park & Ostriker 1989; Park 1990a; NTZ). We stress that in all the discussion leading to the equation for T_{γ} , we assumed a non-relativistic distribution for electrons. This has been done to ensure consistency with the Compton source term which has the simple expression given in equation (23) only in the non-relativistic limit.

Finally, we need to specify the constitutive equations for a pure hydrogen gas

$$P = [1 + x(T)] \frac{\rho k_B T}{m_p}, \quad (32)$$

$$e = \rho c^2 \left\{ 1 + \frac{3}{2} [x(T) + x^*(T)] \frac{k_B T}{m_p c^2} - [1 - x(T)] \frac{E_H}{m_p c^2} \right\}, \quad (33)$$

where T is the gas temperature, $E_H = 13.6$ eV is the hydrogen ionization potential and $x(T)$ is the degree of ionization, computed by equating the collisional-ionization and radiative-recombination rates (Buff & McCray 1974) and expressed using the interpolation formula of Stellingwerf and Buff (1982)

$$x(T) = \frac{F}{1 + F}, \quad (34a)$$

with

$$F = 2 \left(\frac{T}{1 \text{ K}} \right) \exp \left(\frac{-1.58 \times 10^5 \text{ K}}{T} \right).$$

In equation (33)

$$x^*(T) = \frac{2}{3} [\theta^{-1}(\eta - 1) - 1], \quad (34b)$$

where $\theta = k_B T / m_e c^2$ and $\eta = K_3(\theta^{-1}) / K_2(\theta^{-1})$ (K_n is the modified Bessel function of order n). A polynomial fit by Service (1986) was used to calculate η , giving an accuracy of a few parts in 10^5 . The third term inside the curly brackets in equation (33) accounts for the electrostatic potential energy of bound electrons in the neutral hydrogen atoms.

The constitutive equations (32) and (33) can be used to express two fluid variables in terms of the other ones. Since the values of the temperature T and the density ρ are needed for evaluating the source moments s_0 and s_1 , it is more convenient to use them in the hydrodynamic equations and to calculate e and P from equations (32) and (33). Substituting equation (33) into equation (15), the Energy equation can be written in the form

$$\left[\frac{3}{2} (x + x^*) + \left(\frac{3}{2} + \frac{E_H}{k_B T} \right) \frac{dx}{d \ln T} + \frac{3}{2} \frac{dx^*}{d \ln T} \right] \frac{k_B T}{m_p c^2} \frac{T_t}{T} + P \left(\frac{1}{\rho} \right)_t + \frac{a s_0}{\rho} = 0. \quad (35)$$

As far as the closure function is concerned, in the present calculation we chose to relate w_2 to w_0 using the following expression

$$f = \frac{w_2}{w_0} = \frac{2}{3} \left[1 + \left(\frac{\tau}{\tau_0} \right)^n \right]^{-1}, \quad (36)$$

where τ_0 and n are free parameters. We made several trials with different expressions for f and found that the fractional difference between solutions obtained with different reasonable closures turns out to be no larger than $\sim 20\%$, which is acceptable here. In fact, a change in the closure parameters was used to perturb the initial stationary solution, as we will discuss later.

4 BOUNDARY CONDITIONS

From the mathematical point of view, the equations of radiation hydrodynamics (16)–(21) and (35), the first two moment equations (22) and the radiation temperature equation (30) form a hyperbolic system. In order for the problem to

Table 1. Parameters for the Stationary Models.

| | \dot{m} | l | $\eta = l/\dot{m}$ |
|----|-----------|----------------------|----------------------|
| 1L | 28.5 | 4.8×10^{-6} | 1.7×10^{-7} |
| 2L | 4.27 | 9.2×10^{-7} | 2.2×10^{-7} |
| 3L | 0.071 | 3.5×10^{-8} | 4.9×10^{-7} |
| 0H | 70.8 | 7.3×10^{-3} | 1.0×10^{-4} |
| 1H | 28.3 | 1.4×10^{-3} | 5.0×10^{-5} |
| 2H | 3.45 | 2.2×10^{-4} | 6.5×10^{-5} |

be well-posed, we need to specify values for all of the variables at some initial time $t = t_0$ over all of the integration domain $\mu_{in} \leq \mu \leq \mu_{out}$ and also to assign suitable boundary conditions at the spatial boundaries μ_{in}, μ_{out} . The number of boundary conditions needed depends on the sign of the eigenvalues of the characteristic equations at each boundary. At the outer boundary, negative eigenvalues signify that information is propagating into the integration domain from outside and a corresponding number of conditions must be assigned; the same is true for positive eigenvalues at the inner boundary. In the present case it can be shown that we need to prescribe 7 boundary conditions (4 at the inner boundary and 3 at the outer boundary) as follows: 2 conditions related to the fluid equations, 2 related to the moment equations, 1 each for the equations for T_γ , a and M . As far as the fluid boundary conditions are concerned: at $\mu = \mu_{out}$ we set a floating boundary (extrapolation in r) for u and, at $\mu = \mu_{in}$, we dropped the pressure gradient term from the Euler equation, making it advective in form and assuming strict free-fall very near to the black hole horizon. The inner conditions on T_γ and w_1 and the outer condition on w_0 were all taken as floating boundaries. The choice of a floating boundary is suitable when one does not want to put any constraint on a variable, leaving it free to adjust itself or to oscillate if there are waves propagating out of the integration domain (as for a vibrating string with free endpoints).

As far as a and M are concerned, the time-slice at constant t is a characteristic direction for equations (19) and (20) and we put

$$a = 1 \quad \text{at } \mu = \mu_{out}, \quad (37)$$

$$M = M_0 \quad \text{at } \mu = \mu_{in}. \quad (38)$$

The condition on a , equation (37), corresponds to synchronizing the coordinate time with the proper time of a comoving observer at the outer edge of the grid. This is also equal to the Eulerian time there, if the outer edge of the grid is placed sufficiently far away from the black hole.

Finally, we note that, if the system tends to a stationary limit, the time-dependent equations reduce to their stationary form and the solution which crosses any critical points in a regular way is automatically selected.

5 NUMERICAL METHOD

The equations of radiation hydrodynamics, presented in sections 2 and 3, have been solved numerically for matter being accreted spherically onto a Schwarzschild black hole, using a Lagrangian finite difference scheme with a standard Lagrangian organization of the grid. The code was adapted from one developed by Miller & Rezzolla (1995) for solution of the equations of radiation hydrodynamics in the context

of the cosmological quark-hadron transition. We divided the integration domain (from the black hole horizon at $r = r_g$ out to $10^9 r_g$) into a succession of comoving zones with each one having width $\Delta\mu$ 21% larger than the one interior to it. Whenever the inner edge of the innermost zone crosses the horizon (which happens every 4–5 cycles with our time-step constraints), we remove it from the calculation and perform a regridding of all the variables. We followed a regridding procedure previously adopted by Szuszkiewicz & Miller (1995) in connection with the study of disc accretion onto black holes. Originally a cubic spline interpolation was used, but this turned out to produce a numerically unstable evolution in our case. A local cubic interpolation was eventually used instead, which was found to be satisfactory and efficient. At the initial time the effective mass contained within the inner boundary, M_0 , is equal to the initial black hole mass M_{bh} , which we take to be $3M_\odot$ as in the stationary calculations. As time elapses, M_0 increases as zones pass through the horizon and are removed from the calculation. However, during a characteristic evolutionary time interval, the mass of the material accreted is small compared with M_{bh} .

To have second-order accuracy in time, u and w_1 are both evaluated at an intermediate time level. They are advanced to the new time level at the end of each cycle after all of the other variables have been calculated. The time-step is adjusted in accordance with the relativistic Courant condition and two additional constraints on the fractional variations of ρ and T in each time-step, which are required to be smaller than 5%. In practice, we found that the time-step is usually limited by the last two conditions due to the fact that the variation of density and temperature, as seen by comoving observers, becomes very rapid near to the horizon where the flow velocity approaches the speed of light. As far as the spatial centering is concerned, ρ, T, w_0, T_γ and a are treated as mid-zone quantities, while r, M, u and w_1 are treated as zone boundary quantities.

Once the finite difference representation has been introduced, equations (16), (17), (19), (20) and (21) can be solved explicitly for u, ρ, a, M and r , respectively. Where necessary, linear interpolation and extrapolation in time were used to obtain the values of quantities at suitable time levels. The semi-logarithmic derivatives present in the Continuity equation (17) and the equation for a (19) were solved using the Crank–Nicholson operator for equation (17) and the Leith–Hardy operator for equation (19) (see e.g. May & White 1967). For the moment equations (22), we adopted a mixed representation: after dividing the first equation by w_0 and the second by w_1 we grouped together the terms in the following way:

$$\frac{(w_0)_t}{w_0} = - \left[\frac{4}{3} \left(\frac{b_t}{b} + 2 \frac{r_t}{r} \right) + \left(\frac{b_t}{b} - \frac{r_t}{r} \right) f \right] + \frac{ac}{w_0} \left[s_0 - \frac{1}{a^2 b r^2} (w_1 a^2 r^2)_\mu \right], \quad (39a)$$

$$\frac{(w_1)_t}{w_1} = - 2 \left(\frac{b_t}{b} + \frac{r_t}{r} \right) + \frac{ac}{w_1} \left[s_1 - \frac{1}{3a^4 b} (w_0 a^4)_\mu - \frac{1}{ab r^3} (f w_0 a r^3)_\mu \right], \quad (39b)$$

where w_2 has been expressed using the closure relation $w_2 = f w_0$ with f being defined as in equation (36). The

Table 2. Time-scales.

| | | |
|---|---------------------------------------|---|
| $t_d = \frac{r}{u_c}$ | dynamical time | |
| $t_{sg} = \frac{r}{v_s c}$ | sound crossing time for the gas | $v_s = \frac{1}{c} \left(\frac{\partial P}{\partial \rho} \right)_s^{1/2}$ |
| $t_{sr} = \frac{r}{v_c c}$ | sound crossing time for the radiation | $v_c = \left(f + \frac{1}{3} \right)^{1/2}$ |
| $t_c = \frac{e - \rho c^2 + P}{C}$ | cooling time | $C = \rho c \left(\epsilon + k_{es} w_0 \frac{4k_B T}{m_e c^2} \right)$ |
| $t_h = \frac{e - \rho c^2 + P}{H}$ | heating time | $H = \rho c w_0 \left(k_0 + k_{es} \frac{4k_B T_\gamma}{m_e c^2} \right)$ |
| $t_{th} = \frac{e - \rho c^2 + P}{ H - C }$ | thermal time | |

terms on the left hand side of equations (39) were treated using the Crank–Nicholson operator, while the quantities appearing on the right hand side were calculated at the correct time level by means of interpolation or extrapolation where necessary. Because the dependence on temperature in the Energy equation is rather sensitive, we adopted a semi-implicit scheme for equation (35) using a secant iteration method. The temperature at the new time level is calculated iteratively starting from two initial estimates, based on the value at the previous time-step. Convergence is rapidly achieved in 4–5 iterations. Since s_0 is in general very sensitive to the value of the temperature, the iteration was extended to include also the zero-th moment equation (39a). The equation for T_γ (equation [30]) presents a particular numerical problem because of the delicate balance between T and T_γ which, following Bowers & Wilson (1991), we treated using a fully implicit differencing for $(T - T_\gamma)$ to achieve numerical stability.

6 NUMERICAL RESULTS AND DISCUSSION

We have calculated the time evolution of 6 models, starting from the stationary solutions listed in table 1 whose position in the (\dot{m}, l) plane is shown in Fig. 1. Because of the different form of the T_γ equation used here, the present stationary solutions differ slightly from those of NTZ (see equation [31] and the following discussion). The definitions of relevant time-scales for the present discussion are listed in table 2. Along with the dynamical time-scale, t_d (which is the characteristic time for an element of fluid with velocity u to travel a distance r), we have listed also the sound crossing times for the gas, t_{sg} , and for the radiation, t_{sr} (these are defined as the ratio of the radial length scale to the relevant characteristic velocity and represent the time needed for a ‘sound’ wave in the gas or radiation fluid to travel a distance r). For determining whether stationary solutions are stable or not, we should in principle evolve each model for a time comparable with the relevant t_{sg} or t_{sr} in order to allow information to travel from the inner regions to the outer ones. At $10^5 r_g$, $t_{sg} \sim 10^4$ s and $t_{sr} \sim 1$ s. To reach an evolutionary time $t = 10^4$ s would require prohibitively high computational times but in fact, as we shall see, all of the models evolve on a much shorter time-scale (typically of a few seconds) which is mainly determined by the thermal and radiative processes. The thermal balance is regulated by the cooling and heating time-scales, t_c and t_h , which are the ratios of the internal energy of the gas to the cooling rate (C) and heating rate (H), respectively, and are both defined in table 2. We have also introduced the thermal time-scale, t_{th} , defined as the ratio of the internal energy of the gas to

the net rate of energy input or output for the gas, $|H - C|$.

For each model we started the numerical calculation from an initial perturbed solution which was calculated by changing the closure function. By varying τ_0 and n in equation (36), we obtained a perturbation of the order of 10–20 % in the gas temperature and in the radiation moments. This way of setting the perturbation was not effective for model 3L, which is optically thin everywhere, and so, only in this case, we decided to evolve the solution without any initial perturbation just to have an indication of the intrinsic stability of these models. The solution after 14 seconds remains exactly in the initial stationary state. This is not surprising since, in this case, we know that cooling is very inefficient and so the result obtained by Moncrief (1980), who found that adiabatic flows are stable, was likely to apply here. In fact, optically thin solutions are not of great interest and we did not spend further time in the numerical analysis of the stability of these models.

In Fig. 2 the results from the numerical calculation for model 1L are shown. This solution is representative of the behaviour of all optically thick LL models. As can be seen from the figure, the solution relaxes toward the stationary state (shown with a continuous line) on a time-scale of the order of t_{th} which, for this solution, is much shorter than 1 second within $10^3 r_g$. This shows that these solutions are stable, in agreement with the result obtained by Vitello (1984). The perturbation does not directly involve velocity and density, which remain essentially equal to their initial values and the accretion rate also remains extremely constant. Radiation and gas pressure have negligible effect in these cases and matter is essentially in free-fall from the sonic radius (located at $r \simeq 10^9 r_g$) down to the black hole horizon. Temperature and luminosity relax very quickly to their stationary values. In the optically thick inner core, matter and radiation are in LTE and the luminosity is proportional to the local value of the temperature gradient; in the outer region compressional heating balances free-bound cooling and the gas is essentially in radiative energy equilibrium at the hydrogen recombination temperature, $T \simeq 10^4 K$.

For models on the high luminosity branch, the behaviour of the time-dependent solutions is completely different. In Figs. 3 and 4, we show the results of numerical calculations for models 2H and 1H, respectively. The matter fluid is essentially in free-fall and the accretion rate is roughly constant. The interpretation of the temperature and luminosity profiles is less straightforward. They do not seem to converge at all toward the stationary solutions found by NTZ, but, after 70 seconds, they are still in essentially the initial perturbed state. We postpone discussion of these solutions to the end of this section.

Figure 2

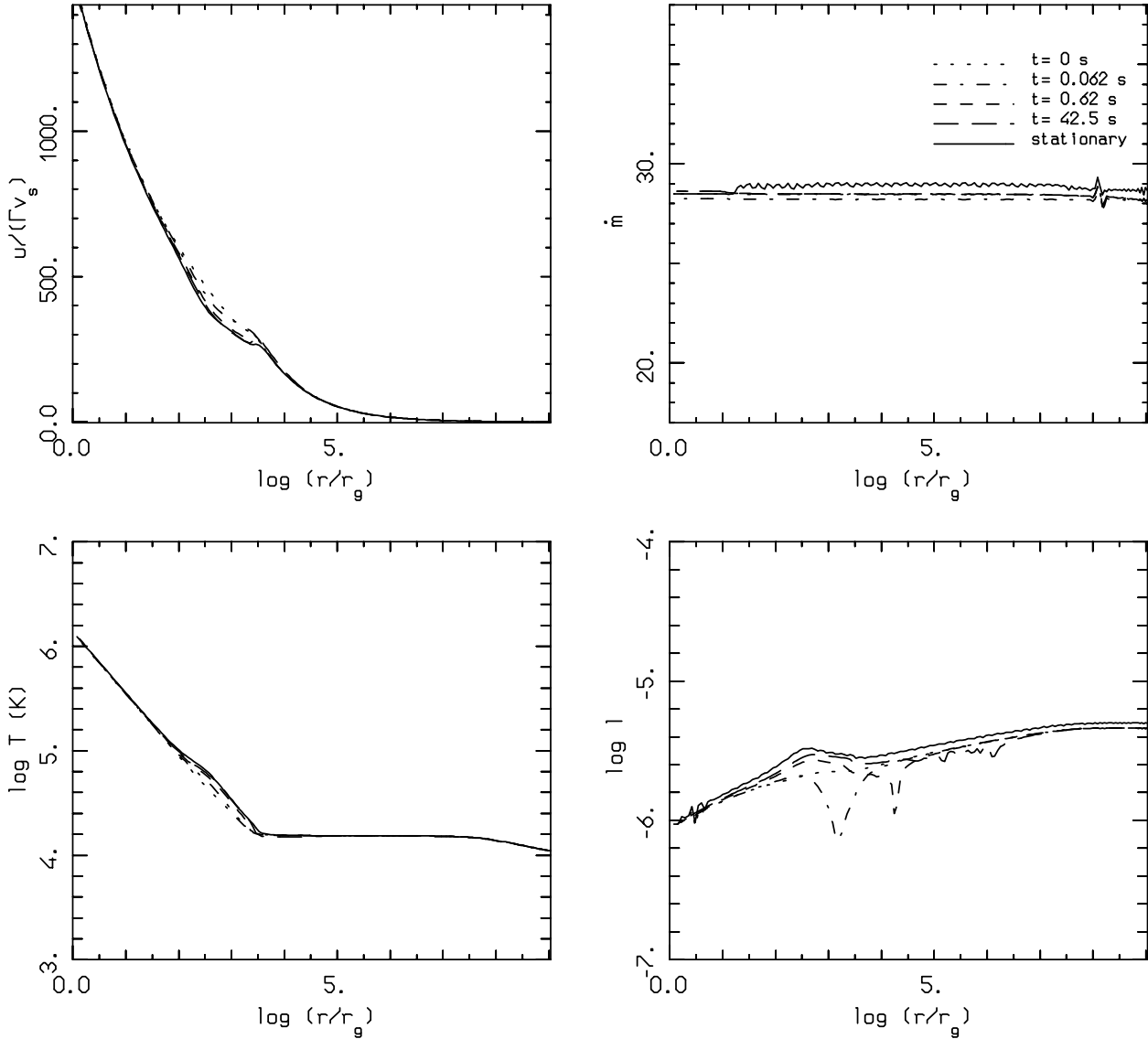
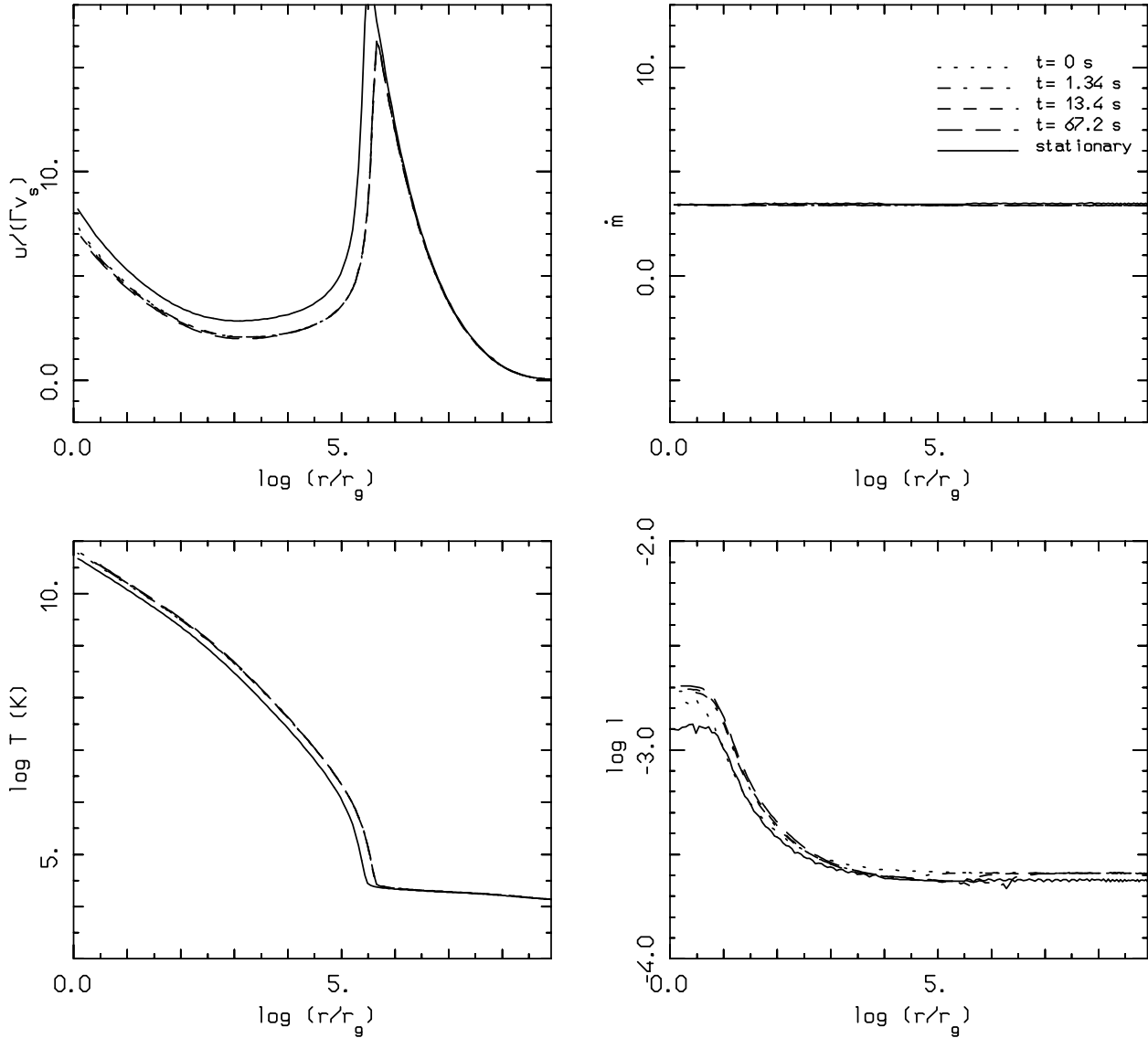


Figure 2. The Mach number $u/\Gamma v_s$, the accretion rate in Eddington units \dot{m} , the gas temperature T and the radiative luminosity $l = 4\pi r^2 c w_1 / L_E$ are plotted versus $\log(r/r_g)$ for model 1L at different times.

For larger \dot{m} (model 1H), a thermal instability appears in the inner part of the flow after about 2–3 seconds, as can be seen from Fig. 4, and the temperature increases by almost an order of magnitude. The cause of the onset of this instability will be discussed later. A few seconds after this, the velocity profile starts to deviate significantly from free-fall owing to the large drag exerted by the internal pressure gradients. A compression wave develops, whose front becomes progressively steeper as it propagates outward and, after 8–10 seconds, a hydrodynamic shock forms at around 10^3 – $10^4 r_g$, where the Mach number passes through unity

(small-dashed line in Fig. 4). Across the shock, the kinetic energy of the gas is dissipated into thermal energy and the density increases; matter starts to accumulate at the shock front and a corresponding decrease in ρ is seen in the inner region. Immediately behind the shock front, the gas accelerates and free-fall is rapidly restored. We note that since the shock is very far away from the black hole horizon, the kinetic energy dissipated there is relatively small and the radiative luminosity does not increase significantly through it. As far as we know, this is the first time that a shock has been found in self-consistent solutions of black hole accretion (see

Figure 3**Figure 3.** The same as Fig. 2 for model 2H.

Chang & Ostriker 1985 for a discussion of shock formation in stationary models). The large increase of l in the first 8–10 seconds (by more than one order of magnitude) is due to the enhancement in efficiency of free–free and Compton cooling caused by the increase in T . At later times, l starts to decrease because of the fall in density which leads to a decrease in efficiency of the cooling processes interior to the shock radius. The luminosity profile then has the typical behaviour shown in Fig. 4 with the long-dashed line. This time variation is seen by a distant observer as a significant initial transient increase lasting ~ 8 s followed by a relatively rapid decrease at later times. Looking carefully at the Mach num-

ber profile, it can be seen that the shock front (where the Mach number falls below one) is moving outward, at an approximate speed of 10^8 cm/s $\simeq 10^{-2}c$. Hence this solution is definitely non-stationary as confirmed by the fact that the accretion rate is not constant and matter keeps accumulating at the shock front. The evolution of model 1H (Fig. 4) was followed inserting a source of artificial viscosity, with the aim of getting a better treatment of the shock region. Following the standard prescription by von Neumann and Richtmyer (1950), a dissipative term $Q \propto \rho_{i-1/2} (u_i - u_{i-1})^2$, was inserted into the equations (here the subscripts indicate the locations on the finite difference grid at which each variable

Figure 4

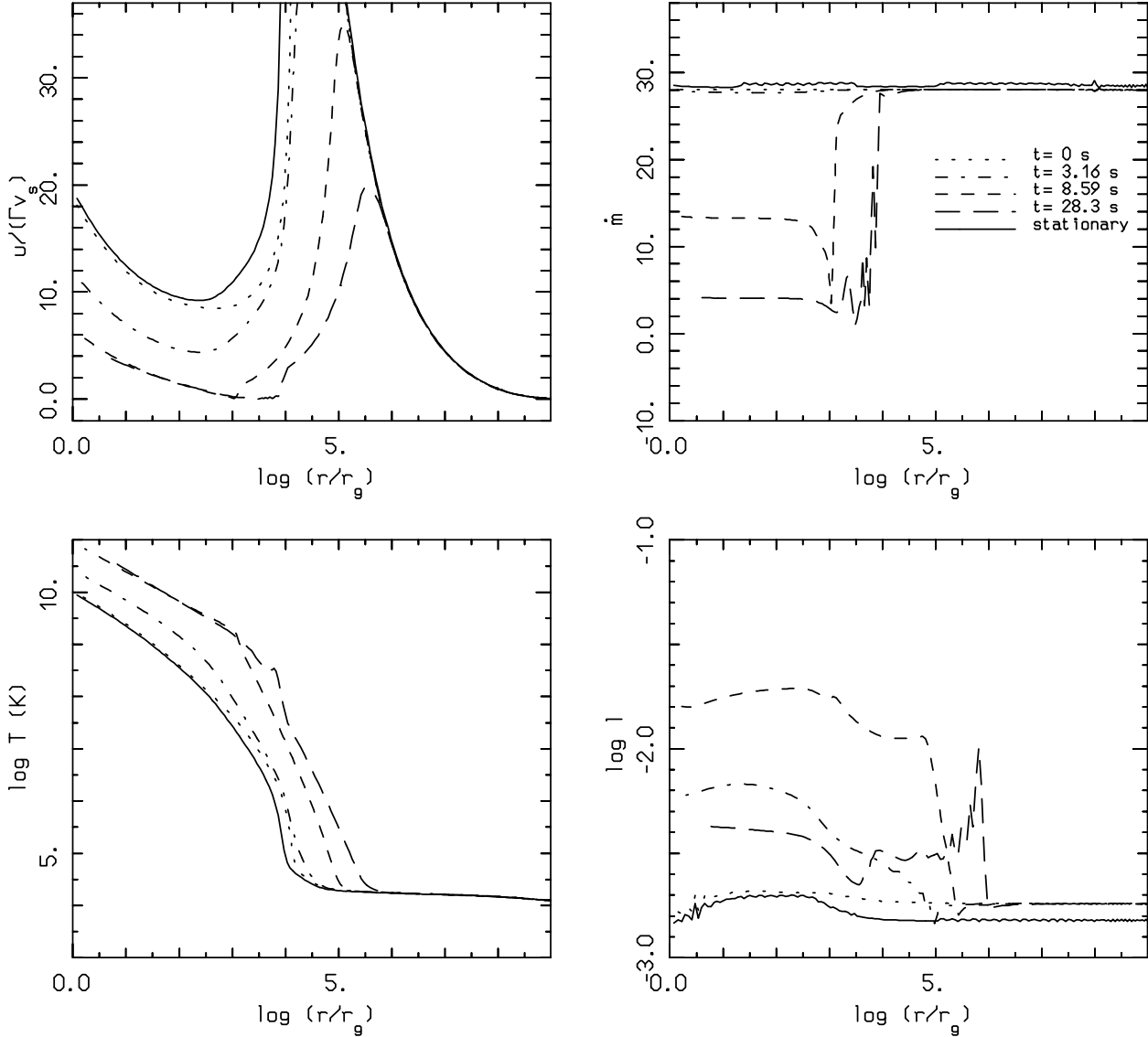


Figure 4. The same as Fig. 2 for model 1H.

is evaluated; i represents a zone boundary and $i - 1/2$ represents a mid-zone). However, since the flow is being compressed continuously from the sonic radius down to the black hole horizon, the amount of dissipation would be excessive, especially in the vicinity of r_g , unless some modification is made to the standard procedure. In view of this, we decided to switch on the artificial viscosity only when the fractional variation of u across a grid zone $\alpha = 2(u_i - u_{i-1})/(u_i + u_{i-1})$ becomes larger than 30%. As the shock forms, α increases above 0.3 and the viscous term

$$Q_{i-1/2} = k \left(1 - \frac{0.3}{\alpha}\right) \rho_{i-1/2} (u_i - u_{i-1})^2 c^2 \quad (40)$$

then starts to be progressively more effective. Here k is an adjustable constant ($k = 2$ in the actual calculation). About 30 seconds after the beginning of the evolution and approximately 20 seconds after the shock formation, we were nevertheless forced to stop the calculation because of the formation of large numerical oscillations at the shock front and some more sophisticated treatment would clearly be desirable. However, for the present purposes, we were content simply to demonstrate the existence of the shocked solutions.

The evolution described for model 1H, with the appearance of a thermal instability and the formation of a hydro-

dynamic moving shock, is a common feature of all of the high luminosity models along the high \dot{m} part of the HL branch. We have made a systematic search for the point on the (\dot{m}, l) plane which marks the onset of the instability and the result is shown in Fig. 1, where all of the HL unstable models are plotted as open circles. According to the analysis of Field (1965) and Stellingwerf (1982), the form of the free-free cooling function implies that the gas should be thermally unstable to isobaric short-wavelength perturbations so that, if the Compton heating rate exceeds the cooling rate at some radius, it will continue to do so until matter there has been heated to a temperature which is essentially equal to that of the radiation. In the present case, owing to the large value of the Compton parameter Y_c , Compton cooling is equally as efficient as Compton heating and the analysis by Stellingwerf (1982) does not strictly apply. However, as discussed by Cowie, Ostriker & Stark (1978), the instability is clearly due to the fact that the heating rate is greater than the cooling rate and, at the same time, the heating time is shorter than the dynamical time. In Figs. 5 and 6, we have plotted the ratios of the heating time (t_h) to the cooling time (t_c) and of the thermal time (t_{th}) to the dynamical time (t_d). These quantities are plotted against r/r_g at different times for models 2H and 1H, respectively.

As can be seen from Fig. 6, at the beginning t_h is slightly smaller than t_c in the region around 10^3 – $10^4 r_g$. There, heating exceeds cooling and, since the flow cannot advect the excess energy efficiently ($t_d \simeq t_{th}$), a small perturbation is sufficient to make heating more effective and the onset of a thermal instability is unavoidable. Also the value of the thermal time-scale, $t_{th}(10^3 r_g) \sim t_d(10^3 r_g) \sim 1$ s, is consistent with the time-scale for the onset of the instability found numerically. The region of instability then moves to larger radii, as can be seen from Fig. 6, and so it is not surprising that the shock keeps moving outward. On the other hand, Fig. 5 shows that the ratio t_{th}/t_d is significantly larger than unity for model 2H in the region where heating is more effective than cooling and so the thermal instability is advected into the hole on a dynamical time-scale. In other words, since the models along the low \dot{m} part of the HL branch have smaller gas densities, the radiative heating and cooling are comparatively less efficient than compressional heating and the gas is essentially adiabatic. Only very far away, around $3 \times 10^5 r_g$, do the conditions seem to be favourable for the onset of the thermal instability; however, the thermal time-scale in that region is $\sim 10^3$ s and the evolutionary time becomes very large. This means that these solutions might also be unstable but on much longer time-scales.

Finally, we note that, during the evolutionary times considered, we did not find any evidence for possible transitions between the HL and the LL branch.

7 CONCLUSIONS

We have presented a systematic analysis of the stability and time-dependent behaviour of spherical accretion onto black holes in the framework of general-relativistic radiation hydrodynamics. We have computed the evolution of a number of models from an initial perturbed state and confirmed that all of the low luminosity, NTZ stationary solutions, which are characterized by negligible comptonization, are indeed stable to thermal and radiative perturbations in agreement

with previous investigations (e.g. Gilden & Wheeler 1980; Vitello 1984). On the other hand, the time evolution of high luminosity solutions, for which self-comptonization of bremsstrahlung photons is the main radiative and thermal process, exhibits a much richer phenomenology. We find that the upper part of the HL branch (for $\dot{m} \gtrsim 10$) enters the region of the (\dot{m}, l) plane where preheating effects start to be important and this leads to the onset of a strong thermal instability giving rise to the formation of an outward-propagating hydrodynamic shock. These shocked solutions show significant transient increases in the total luminosity.

ACKNOWLEDGEMENTS

We gratefully acknowledge helpful discussions with Luciano Rezzolla, Alan Ball and Henk Spruit.

REFERENCES

Begelman, M.C. 1978, A&A, 70, 583
 Begelman, M.C. 1979, MNRAS, 187, 237
 Bisnovatyi-Kogan, G.S., & Blinnikov, S.I. 1980, MNRAS, 191, 711
 Blumenthal, G.R., & Mathews, W.G. 1976, ApJ, 203, 714
 Blondin, J.M. 1986, ApJ, 308, 755
 Bondi, H. 1952, MNRAS, 112, 195
 Bowers R.L., & Wilson J.R. 1991, *Numerical Modeling in Applied Physics and Astrophysics*, (Boston: Jones & Bartlett Publishers)
 Brinkmann, W. 1980, A&A, 85, 146
 Buff, J., & McCray, R. 1974, ApJ, 189, 147
 Cernohorsky, J., & Bludman, S.A. 1994, ApJ, 433, 250
 Chandrasekhar, S. 1960, *Radiative Transfer*, (New York: Dover)
 Chang, K.M., & Ostriker, J.P. 1985, ApJ, 288, 428
 Cowie, L.L., Ostriker, J.P., & Stark, A.A. 1978, ApJ, 226, 1041
 Field, G.B. 1965, ApJ, 142, 431
 Flammang, R.A. 1982, MNRAS, 199, 833
 Flammang, R.A. 1984, MNRAS, 206, 589
 Freihofer, D. 1981, A&A, 100, 178
 Fu, A. 1987, ApJ, 323, 227
 Gilden, D.L., & Wheeler, J.C. 1980, ApJ, 239, 705
 Gillman, A.W., & Stellingwerf, R.F. 1980, ApJ, 240, 235
 Kafka, P., & Mészáros, P. 1976, Gen. Rel. Grav., 7, 841
 Krolik, J.H. & London, R.A. 1983, ApJ, 267, 18
 Maraschi, L., Reina, C., & Treves, A. 1974, A&A, 35, 389
 May, M.M., & White, R.H. 1967, *Methods in Computational Physics*, Vol. 7, Alder, B., Fernbach, S. & Rotenberg, M. eds., (New York: Academic Press)
 Mészáros, P. 1975, A&A, 44, 59
 Michel, F.C. 1972, Ap&SS, 15, 153
 Mihalas, D., & Weibel Mihalas, B. 1984, *Foundations of Radiation Hydrodynamics* (Oxford: Oxford University Press)
 Miller, J.C., & Rezzolla, L. 1995, Phys. Rev. D, 51, 4017
 Moncrief, V. 1980, ApJ, 235, 1083
 Nobili, L., Calvani, M., & Turolla, R. 1985, MNRAS, 214, 161
 Nobili, L., Turolla, R., & Zampieri, L. 1991, ApJ, 383, 250, (NTZ)
 Novikov, I.D., & Thorne, K.S. 1973, in *Black Holes* DeWitt, C., & DeWitt, B.S. eds., p. 343, (New York: Gordon & Breach)
 Ostriker, J.P., McCray, R., Weaver, R., & Yahil, A. 1976, ApJ, 208, L61
 Park, M.-G., & Ostriker, J.P. 1989, ApJ, 347, 679
 Park, M.-G. 1990a, ApJ, 354, 64
 Park, M.-G. 1990b, ApJ, 354, 83
 Park, M.-G. 1993, A&A, 274, 642
 Rees, M.J. 1978, Phys. Scripta, 17, 193

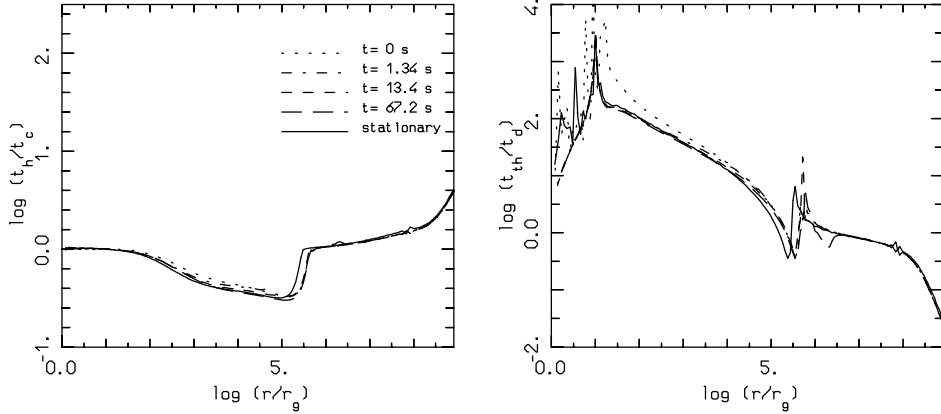
Figure 5


Figure 5. Ratios of the heating time (t_h) to the cooling time (t_c) and of the thermal time (t_{th}) to the dynamical time (t_d) plotted against $\log(r/r_g)$ for model 2H at different times.

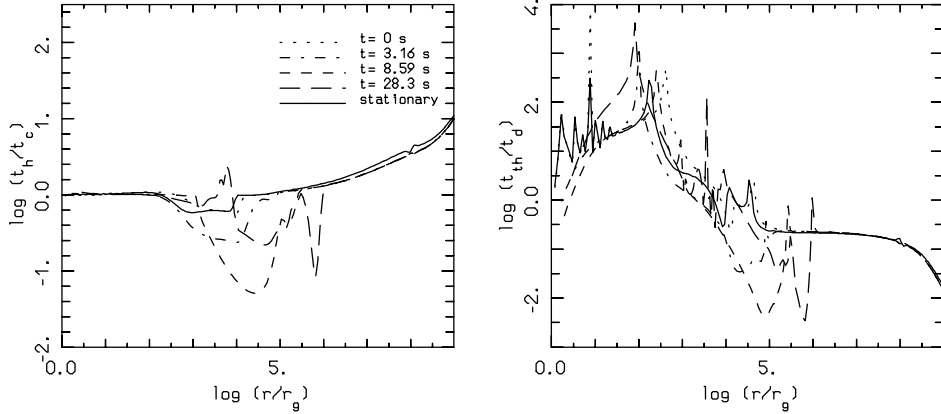
Figure 6


Figure 6. The same as Fig. 5 for model 1H. Note that the curve for $t = 0$ in the left panel is difficult to see because it is almost completely hidden by the continuous line.

Rezzolla, L., & Miller, J.C. 1994, *Class. Quantum Grav.*, 11, 1815
 Rybicki, G.B., & Lightman, A.P. 1979, *Radiative Processes in Astrophysics* (New York: Wiley)
 Schmid-Burgk, J. 1978, *Ap&SS*, 56, 191
 Service, A.T. 1986, *ApJ*, 307, 60
 Shapiro, S.L. 1973a, *ApJ*, 180, 531
 Shapiro, S.L. 1973b, *ApJ*, 185, 69
 Shull, J.M. 1979, *ApJ*, 229, 1092
 Shvartsman, V.F. 1971, *Soviet Astr.-AJ*, 15, 377
 Soffel, M.H. 1982, *A&A*, 116, 111
 Stellingwerf, R.F., & Buff, J. 1978, *ApJ*, 221, 661
 Stellingwerf, R.F., & Buff, J. 1982, *ApJ*, 260, 755
 Stellingwerf, R.F. 1982, *ApJ*, 260, 768
 Szuszkiewicz, E., & Miller J.C. 1995, in preparation
 Tamazawa, S., Toyama, K., Kaneko, N., & Ôno, Y. 1974, *Ap&SS*, 32, 403

Thorne, K.S. 1981, *MNRAS*, 194, 439
 Turolla, R., & Nobili, L. 1988, *MNRAS*, 235, 1273
 Vitello, P.A.J. 1978, *ApJ*, 225, 694
 Vitello, P.A.J. 1984, *ApJ*, 284, 394
 von Neumann, J., & Richtmyer, R.D. 1950, *J. Appl. Phys.*, 21, 232
 Wandel, A., Yahil, A., & Milgrom, M. 1984, *ApJ*, 282, 53

APPENDIX A

As discussed in the text, we take equation (28) to be valid along the outward-pointing characteristics of the radiation field, $\mu_c(t)$, with the optical depth being defined along the

same lines by

$$\tau = \int_{\mu}^{\infty} k_{es} \rho b \Gamma d\mu. \quad (\text{A1})$$

Then, we have

$$\frac{d\tau}{d\mu} = -k_{es} \rho b \Gamma. \quad (\text{A2})$$

(Throughout this Appendix the total derivatives are taken along the outward-pointing characteristics of the radiation field). Using equations (A2) and (28), we can write

$$\begin{aligned} \frac{dT_{\gamma}}{dt} &= \frac{dT_{\gamma}}{d\tau} \frac{d\tau}{d\mu} \dot{\mu}_c = -k_{es} \rho b \Gamma \dot{\mu}_c \frac{dT_{\gamma}}{d\tau} \\ &= -ac \Gamma v_c \frac{2k_{es} \rho Y_c}{\tau} T_{\gamma} \left(\frac{T_{\gamma}}{T} - 1 \right), \end{aligned} \quad (\text{A3})$$

where $\dot{\mu}_c = d\mu_c/dt$ and $v_c = b\dot{\mu}_c/ac = (f + 1/3)^{1/2}$. However, also

$$\frac{dT_{\gamma}}{dt} = \frac{\partial T_{\gamma}}{\partial t} \Big|_{\mu} + \frac{\partial T_{\gamma}}{\partial \mu} \Big|_t \dot{\mu}_c \quad (\text{A4})$$

and so we finally get

$$\frac{\partial T_{\gamma}}{\partial t} \Big|_{\mu} = -ac \Gamma v_c \left[\frac{2k_{es} \rho Y_c}{\tau} T_{\gamma} \left(\frac{T_{\gamma}}{T} - 1 \right) + \frac{1}{b\Gamma} \frac{\partial T_{\gamma}}{\partial \mu} \Big|_t \right]. \quad (\text{A5})$$

In practice, we obviously cannot calculate the integrated value of τ directly from expression (A1) evaluated along the outward-pointing characteristics for the radiation since this would involve knowledge of information ahead of the current time reached in the calculation. Instead, we evaluated equation (A1) along the time-slice and this should give reasonable values. While it is important to calculate the *derivative* (A2) along the correct directions in order to ensure a satisfactorily causal propagation of information, the calculation of the *integral* (A1) should not be so sensitive.

To derive the stationary limit of equation (A5), we need first to write it in terms of the Eulerian time and radial coordinates (\tilde{t}, r) . Using the chain rule for differentiation in equation (A5), we obtain

$$\begin{aligned} \tilde{t}_t \frac{\partial T_{\gamma}}{\partial \tilde{t}} \Big|_r + r_t \frac{\partial T_{\gamma}}{\partial r} \Big|_{\tilde{t}} &= -ac \Gamma v_c \left[\frac{2k_{es} \rho Y_c}{\tau} T_{\gamma} \left(\frac{T_{\gamma}}{T} - 1 \right) \right. \\ &\quad \left. + \frac{1}{b\Gamma} \tilde{t}_\mu \frac{\partial T_{\gamma}}{\partial \tilde{t}} \Big|_r + \frac{1}{b\Gamma} r_\mu \frac{\partial T_{\gamma}}{\partial r} \Big|_{\tilde{t}} \right]. \end{aligned} \quad (\text{A6})$$

The condition of stationarity is expressed with respect to the fixed (constant r) Eulerian observer by

$$\frac{\partial}{\partial \tilde{t}} \Big|_r = 0. \quad (\text{A7})$$

Taking the stationary limit in equation (A6) and using $r_t = acu$ and $r_\mu = b\Gamma$ finally yields

$$\left(1 + \frac{u}{\Gamma v_c} \right) \frac{\partial T_{\gamma}}{\partial r} \Big|_{\tilde{t}} = -\frac{2k_{es} \rho Y_c}{\tau} T_{\gamma} \left(\frac{T_{\gamma}}{T} - 1 \right), \quad (\text{A8})$$

which corresponds to equation (31).